CrystEngComm

Streams, cascades, and pools: Various water cluster motifs in structurally similar Ni(II) complexes

Journal:	*CrystEngComm*
Manuscript ID	CE-ART-07-2018-001153.R2
Article Type:	Paper
Date Submitted by the Author:	09-Oct-2018
Complete List of Authors:	Saraei, Nina; University of Louisville, Department of Chemistry Hietsoi, Oleksandr; University of Louisville, Department of Chemistry Mullins, Christopher; University of Louisville, Department of Chemistry Gupta, Alexander; University of Louisville, Department of Chemical Engineering Frye, Brian; University of Louisville, Department of Chemistry Mashuta, Mark; University of Louisville, Department of Chemistry Buchanan, Robert; University of Louisville, Department of Chemistry Grapperhaus, Craig; University of Louisville, Department of Chemistry

Please do not adjust margins

Journal Name

ARTICLE

Streams, cascades, and pools: Various water cluster motifs in structurally similar Ni(II) complexes

Received 00th January 20xx,
Accepted 00th January 20xx

DOI: 10.1039/x0xx00000x

www.rsc.org/

Nina Saraei,[1] Oleksandr Hietsoi,[1] Christopher S. Mullins,[1] Alexander J. Gupta,[2] Brian C. Frye,[1] Mark S. Mashuta,[1] Robert M. Buchanan,[1]* Craig A. Grapperhaus[1]*

Hydrogen bonding (HB) interactions are well known to impact the properties of water in the bulk and within hydrated materials. A series of Ni(II) complexes based on chelates containing *N*-(2-aminoethyl)-1-methylimidazole-2-carboxamide have been synthesized and fully characterized by single crystal x-ray diffraction, spectroscopic methods, and thermal analysis. The complexes reveal a variety of water cluster motifs dependent on the packing arrangement in the solid state. A key feature is the orientation of the carboxamide moiety, which leads to the formation of void spaces that accommodate water through HB interactions. The water motifs contain 1D water chains (streams), 2D tapes of infused rings (cascades), and isolated water dimers (pools). The HB motifs in the hydrated structures vary as a function of the crystal packing of the host molecules. Thermal analyses show a correlation between the HB motif in the hydrated crystals and the temperature range of the dehydration process. The conductivity of the hydrated crystals varies as a function of the crystal packing interactions between metal complexes.

Introduction

The structure and properties of water in confined environments continues to attract attention due its fundamental importance in our understanding of biological, chemical, and physical processes.[1] For example, the dielectric constant value for water decreases dramatically when it is confined in small spaces.[2] The physical properties of water are influenced by the connectivity of hydrogen bonding (HB) networks and dimensionality of void spaces within host environments associated with 1D,[3] 2D,[4] and 3D[5] supramolecular porous materials. In addition, many pharmaceuticals exist as crystalline hydrates that are important requirements to maintain chemical and physical stability.[6]

Much effort has been devoted to the design and engineering of host environments that stabilize discreet water clusters of varying sizes and shapes.[7-9] HB fluctuations within these systems have been evaluated both experimentally[10] and theoretically[11] to provide insight into the structure and properties of confined water in solids. Structures containing 1D water wires are of particular interest because of their presence in many biological systems.[12] Most notably, 1D waters are involved in proton and water transport.[13] For example, in the membrane protein gramicidin A (gA), protons are envisioned to hop along a water wire according to the Grotthhuss relay mechanism[14] or migrate along the chain as ionic water clusters ($H_9O_4^+$ or $H_5O_2^+$).[15]

In this study, we will examine changes in water HB patterns for a group of structurally related hydrated Ni(II) complexes containing N_3X (X = S or O) donors, Scheme 1. Small changes in the ligand framework result in different orientations of the carboxamido oxygens, which influences the solid state packing and HB patterns. Three different network structures are observed including 1D water chains (streams), 2D tapes of infused rings (cascades), and isolated water dimers (pools).

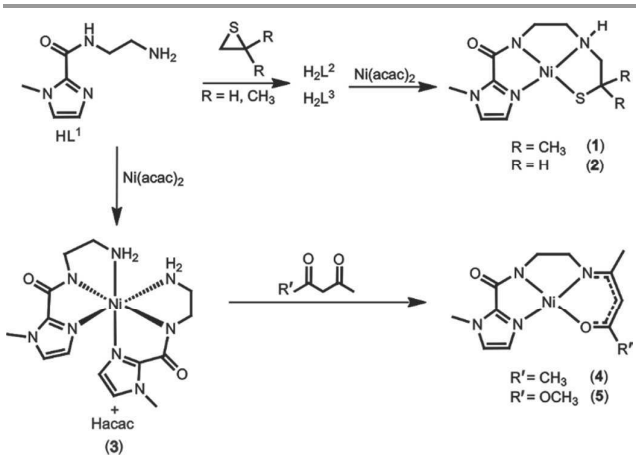

Scheme 1. Synthetic pathways for complexes **1** – **5**.

[1]*Department of Chemistry, University of Louisville, Louisville, 40292, USA.*
[2]*Department of Chemical Engineering, University of Louisville, Louisville, 40292, USA.*

Electronic Supplementary Information (ESI) available: ^{1}H NMR, FT-IR, and MALDI-TOF spectra, unit cell diagrams, TGA and DSC thermal data, conductivity measurements, and selected HB motifs are included in PDF. CIF files have been deposited at the Cambridge Crystallographic Data Centre (1855263-1855266) See DOI:10.1039/x0xx00000x

This journal is © The Royal Society of Chemistry 20xx

Please do not adjust margins

Results and discussion

Synthesis and characterization

A series of Ni(II) compounds, **1** – **5**, based on a *N*-(2-aminoethyl)-1-methylimidazole -2-carboxamide (HL^1) core were synthesized as shown in Scheme 1. The N_3S chelate H_2L^2 and its nickel complex **1** were prepared as previously reported.[16] Similar methods were employed to yield the new chelate H_2L^3 and **2**. Complex **3** was isolated from a mixture of compounds formed upon addition of HL^1 to $Ni(acac)_2$ in dry toluene. Addition of acetone/water or methyl acetylacetate/water to the mixture containing **3** yields complexes **4** or **5**, respectively.

The UV-Vis spectra of **2** – **5** were recorded in acetonitrile or dichloromethane, Figure S6 – S9. The spectrum of **2** is similar to that previously reported for the square planar complex **1** with charge transfer bands at 368, 449, and 575 nm.[16] In contrast, the electronic spectrum of **3** shows low intensity d-d transitions at 488 and 980 nm consistent with an octahedral environment. The spectrum of **4** displays absorbances at 216, 324, 426, and 508 nm assigned to charge transfer bands. Similarily, **5** has bands as at 209, 250, 305, 380, and 475 nm.

The FT-IR spectra of **1** – **5** were collected on solid samples by attenuated total reflectance (ATR correction). The spectra of **1** – **5** show distinct C-N and C=O stretches associated with the carboxamide moiety that are shifted relative to HL^1 due to deprotonation, Table S1. The $\nu_{C=O}$ stretches in **1** and **2** are identical, 1660 cm^{-1}. There is a slight shift to 1610 and 1590 cm^{-1} in **4** and **5**, respectively. For complexes **1** – **3**, the amine N-H stretching frequencies are observed in the range of 3200 – 3300 cm^{-1}. The absence of spectral features between 2400 – 2600 cm^{-1} indicates the thiol group has been deprotonated upon Ni(II) coordination in complexes **1** and **2**. A $\nu_{C=N}$ stretch is clearly visible at 1590 cm^{-1} and 1585 cm^{-1} in complexes **4** and **5**, respectively. In **5**, a medium-strength peak at 1050 cm^{-1} is consistent with the presence of a C-O-CH_3 bond.

Crystallographic studies

Crystal data and structure refinement details for **2** – **5** are listed in Table 1. The structure of **1** has previously been reported.[16] Crystals of **1** – **5** include water of hydration through HB interactions with the metal-ligand complex. A summary of bond distances and angles for **1** – **5** are listed in Table 2 with a summary of HB metric parameters provided in Table 3.

Complex **2** crystallizes as an orange cube that is structurally similar to **1**. Both complexes are in the monoclinic space group $P2_1/c$. The asymmetric unit of **2** contains one equivalent of NiL^2 and a disordered water of hydration, Figure 1. The Ni is coordinated in a pseudo-square planar environment defined by the N_3S chelate with metric parameters similar to **1**. The water of hydration is modeled with a full occupancy oxygen, O2, and one full occupancy hydrogen, H2oa. The remaining hydrogen atom is positionally disordered with 50% occupancy each for H2ob and H2oc.

The water of hydration in **2** participates in three HB interctions. The first is with the carboxamide oxygen O1 of the metal complex in the asymmetric unit. The H-bond is nearly linear with an O2-H2oa···O1 angle of 175(6)°. The donor-acceptor (D···A) and hydrogen-acceptor (H···A) distances of 2.818(4) and 1.93(3) Å, respectively, are consisent with a strong interaction. The two additional H-bonds are to symmetry generated water molecules; O2-H2ob···$O2^{i}$ (-x, -y, -z) and O2-H2oc···$O2^{ii}$ (-x, 1-y, -z).

The extended HB network in **2** can be described as a 1D zig-zag chain of water along the b direction that is anchored to stacked metal complexes, Figure 2. Using the graph set notation,[17] the 1D water molecule chain is described as $C^2_2(4)$ (blue dotted line). The $C^2_2(4)$ chains are held between carboxamide oxygens (O1 and $O1^{ii}$) by a $D^3_3(7)$ motif (red dotted line). Further, the Ni complexes stack through a $C^1_1(4)$ chain involving $S1^{iii}$···H4-N4-Ni (green dotted line). A similar network is observed in **1**. The N-H···S HB in **1** and **2** orient the complexes into an AAAA stacking arrangement. Each carbonyl O of the host interacts with a single water molecule, which is confined in 1D channels.

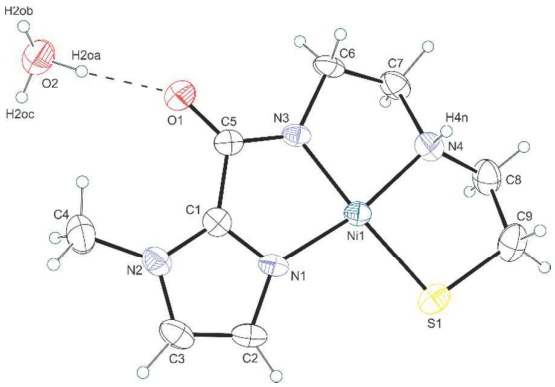

Figure 1. ORTEP[18] representation of the asymmetric unit of NiL^3 (**2**) with thermal ellipsoids shown at the 50% probability level.

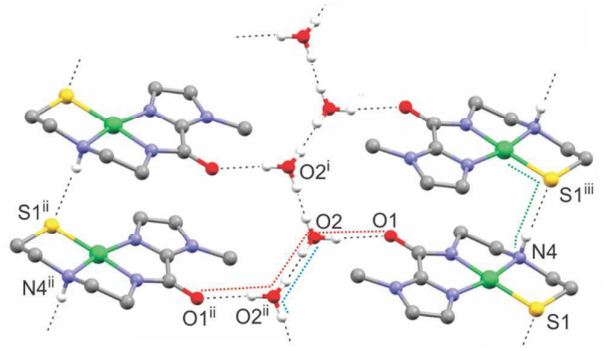

Figure 2. 1D HB "stream" of water in complex **2**. Each O2 atom is bonded to one full occupancy H atom and two partial, 50% occupancy H atoms (see text). HB interactions are denoted by black dashed lines. Graph sets are noted by dotted colored lines as follows: $C^2_2(4)$ (blue); $D^3_3(7)$ (red); $C^1_1(4)$ (green). Atoms generated by symmetry as marked as follows: i = (-x, -y, -z), ii = (-x, 1-y, -z), iii = (x, -1+y,z).

This journal is © The Royal Society of Chemistry 20xx

This journal is © The Royal Society of Chemistry 20xx

Table 1. Crystal data and Structure refinement for **2** – **5**.

identification code	**2**	**3**	**4**	**5**
empirical formula	$C_9H_{14}N_4NiO_1S \cdot H_2O$	$C_{14}H_{22}N_8NiO_2 \cdot H_2O$	$C_{12}H_{16}N_4NiO_2 \cdot 3H_2O$	$C_{12}H_{16}N_4NiO_3 \cdot H_2O$
formula weight	303.03	411.12	361.05	341.01
temperature (K)	100(2)	100(2)	100(2)	100(2)
wavelength (Å)	0.71073	0.71073	0.71073	0.71073
crystal system	Monoclinic	Monoclinic	Triclinic	Monoclinic
space group	$P2_1/c$	$P2/n$	$P\bar{1}$	$P2_1/c$
unit cell dimensions				
a (Å)	11.9515(15)	9.1756(19)	6.8975(18)	9.2792(6)
b (Å)	4.8375(6)	10.590(2)	9.130(2)	13.6005(8)
c (Å)	22.198(3)	9.4434(19)	12.645(3)	21.7240(13)
α (deg)	90.00	90.00	92.821(4)	90.00
β (deg)	103.424(2)	98.876(3)	92.276(4)	95.3700(10)
γ (deg)	90.00	90.00	104.339(4)	90.00
V ($Å^3$)	1248.3(3)	906.7(3)	769.4(3)	2729.6(3)
Z	4	2	2	8
d_{calcd} (Mg/m^3)	1.612	1.506	1.558	1.660
abs coeff (mm^{-1})	1.717	1.103	1.290	1.444
F(000)	632	432	380	1424
cryst size (mm^3)	0.25 × 0.25 × 0.25	0.35 × 0.33 × 0.30	0.50 × 0.03 × 0.01	0.24 × 0.14 × 0.03
ϑ range for data coll. (°)	1.75 to 25.12	2.91 to 25.08	2.90 to 25.11	1.77 to 25.12
index ranges	$-14 \le h \le 14$	$-10 \le h \le 10$	$-8 \le h \le 8$	$-10 \le h \le 11$
	$-5 \le k \le 5$	$-12 \le k \le 12$	$-10 \le k \le 10$	$-16 \le k \le 16$
	$-26 \le l \le 26$	$-11 \le l \le 11$	$-15 \le l \le 15$	$-25 \le l \le 25$
reflns collected	8216	6422	5732	19823
independent reflections	2227 [R(int) = 0.0359]	1621 [R(int) = 0.0141]	2709 [R(int) = 0.0231]	4861 [R(int) = 0.0435]
completeness to theta max	99.4 %	99.9 %	99.1 %	99.8 %
absorption correction	SADABS	SADABS	SADABS	SADABS
max., min transmission	1.000 and 0.636	0.710 and 0.571	0.871 and 0.613	1.000 and 0.754
refinement method	full-matrix least-squares on F^2	full-matrix least-squares on F^2	full-matrix least-squares on F^2	full-matrix least-squares on F^2
data/restrains/params	2227/5/210	1621/0/155	2709/28/257	4861/0/452
goodness of fit on F^2	1.083	1.008	1.052	1.057
final R indices $[I > 2\sigma(I)]^{a,b}$	R1 = 0.0449,	R1 =0.0219,	R1 = 0.0280,	R1 = 0.0364,
	wR2 = 0.1148	wR2 = 0.0567	wR2 = 0.0579	wR2 = 0.0593
R indices (all data)^{a,b}	R1 = 0.0472,	R1 =0.0222,	R1 = 0.0356,	R1 = 0.0561,
	wR2 = 0.1164	wR2 = 0.0569	wR2 = 0.0588	wR2 = 0.0628
largest diff. peak and hole ($e \cdot Å^{-3}$)	0.900 and – 0.458	0.308 and – 0.280	0.394 and – 0.331	0.601 and – 0.302

^{a} $R1 = \Sigma||F_o| - |F_c||/\Sigma|F_o|$. ^{b} $wR2 = \{\Sigma[w(F_o^2 - F_c^2)^2]/\Sigma[w(F_o^2)^2]\}^{1/2}$, where $w = q/\sigma^2(F_o^2) + (qp)^2$ + bp. GOF = $S = \{\Sigma[w(F_o^2 - F_c^2)^2]/(n-p)\}^{1/2}$, where *n* is the number of reflections and *p* is the number of parameters refined.

Complex **3** crystallizes from acetonitrile as blue plates in the monoclinic space group *P*2/n. The asymmetric unit contains one equivalent of $[L^1]^-$, one Ni atom that sits on the special position (0.75, y, 0.75), and one water of hydration. The Ni is coordinated by two equivalents of $[L^1]^-$ in a pseudo-octahedral N_6 environment, Figure 3. The $[L^1]^-$ ligand serves as a meridional chelate with imidazole (N1), amido (N3), and amino (N4) donors.

The asymmetric unit of **3** also contains an O atom, O2, on a special position (0.25, y, 0.75) associated with the water molecule. The symmetry generated hydrogen atom H2o^{ii} (0.5-x, y, 1.5-z) on O2 serves as an H-bond donor to the carboxamido O1 of the metal complex with an O2-H2o^{ii}···O1 angle of 162.8(19)°. The D···A and H···A distances are 2.7979(13) and 2.010(18) Å, respectively. There is a symmetrically equivalent HB interaction between O2-H2o and O1^{ii} that completes a water bridge between neighboring metal complexes defined as a $C^2_2(10)$ HB motif (green dotted line), Figure 4. The carboxamide also serves as an H-bond acceptor with N4-H4NA to form a $C^2_2(12)$ pattern, Figure S32. There are no water-water interactions in the extended network.

Single crystals of **4** were collected from an acetone/water mixture as orange needles in the triclinic space group *P*-1. Orange plate crystals of **5** in the monoclinic space group $P2_1/c$ were obtained from acetonitrile solution by slow evaporation. The asymmetric unit of **4** contains one equivalent of NiL[4] and three waters of hydration, Figure 5. The asymmetric unit of **5** consists of two, crystallographically distinct equivalents of NiL[5]

This journal is © The Royal Society of Chemistry 20xx

Please do not adjust margins

Table 2. Selected Bond Distances (Å) and Bond Angles (°) for **1** – **5**.

Bonds	1	2	3	4	5
Ni1–N1	1.893(3)	1.885(3)	2.1348(13)	1.9013(19)	1.889(2)
Ni1–N3	1.869(3)	1.863(3)	2.0133(13)	1.8517(18)	1.842(2)
Ni1–N4	1.904(3)	1.892(3)	2.1494(13)	1.8444(19)	1.843(2)
Ni1–S1	2.1810(11)	2.1668(11)			
Ni1–O2				1.8350(15)	1.8578(18)
Ni2–O5					1.8521(18)
Ni2–N5					1.898(2)
Ni2–N7					1.840(2)
Ni2–N8					1.847(2)
N1–Ni1–N3	83.77(12)	83.55(13)	78.50(5)	83.55(8)	83.74(10)
N3–Ni1–N4	85.32(12)	85.30(14)	80.27(5)	86.22(8)	86.21(10)
N1–Ni1–N4	168.94(12)	168.59(15)	158.53(5)	169.67(8)	169.88(10)
N4–Ni1–S1	90.57(9)	90.66(11)			
S1–Ni1–N1	100.47(9)	100.55(10)			
N4–Ni1–O2				97.97(8)	97.53(9)
O2–Ni1–N1				92.25(8)	92.50(9)
N5–Ni2–N7					83.81(10)
N7–Ni2–N8					85.91(10)
N5–Ni2–N8					169.14(10)
N8–Ni2–O5					97.30(9)
O5–Ni2–N5					92.90(9)

and a total of two waters of hydration, Figure 6. The Ni centers of **4** and **5** sit in similar N_3O donor environments arranged in pseudo-square planes. The only difference in the donor ligands is the substitution of the methyl group (C12) in **4** with a methoxy group (O3-C12) in **5**.

The three waters of hydration in **4** are involved in extensive HB interactions, Figure 7. The absence of HB between the host layers of **4** allows an ABAB stacking arrangement. This generates void spaces between alternating layers allowing the host carbonyl O to interact with two water molecules. This allows for multi-dimensional HB motifs. The carboxamido oxygen O1 of the metal complex interacts with the O3 and O4 containing water molecules. The O3-H3oa···O1 angle is 175(2)° with a D···A distance of 2.720(2) Å and an H···A distance of 1.938(18) Å. The O4-H4oa···O1 interaction is similar with an angle of 173(3)°, a D···A distance of 2.803(3) Å, and an H···A distance of 2.01(2) Å. Additionally, the O3 containing water molecule acts as an H-bond donor to $O5^{i}$ (x, y, -1+z) and an H-bond acceptor to $O5^{ii}$ (1-x, -y, 1-z). The O4 containing water molecule has a disordered H-atom, modeled as H4ob and H4oc that participates in HB interactions with $O5^{i}$ and $O4^{iii}$ (2-x, 1-y, -z), respectively.

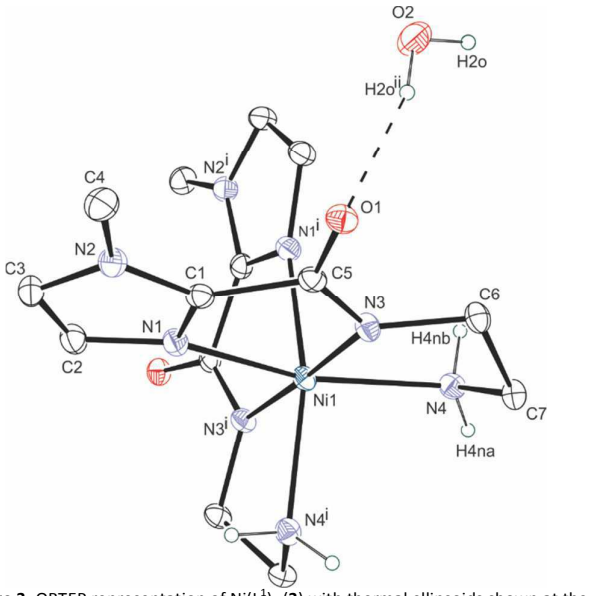

Figure 3. ORTEP representation of $Ni(L^1)_2$ (**3**) with thermal ellipsoids shown at the 50% probability level. Atoms generated by symmetry as marked as follows: i = (1.5-x, y, 1.5-z), ii = (0.5-x, y, 1.5-z).

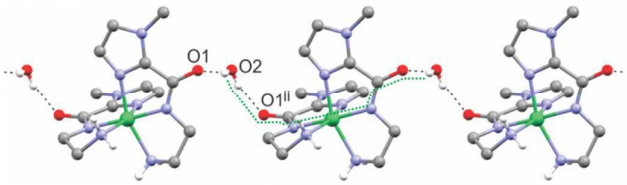

Figure 4. Bridging HB interactions in complex **3**. HB interactions are denoted by black dashed lines. The graph set $C^2_2(10)$ is noted by the dotted green line. Atoms marked with ii are symmetry generated (0.5-x, y, 1.5-z).

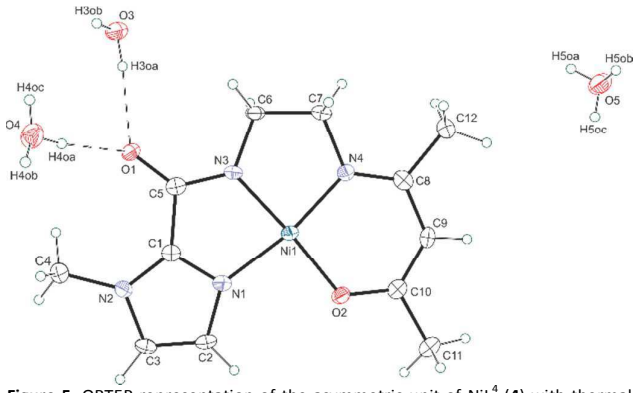

Figure 5. ORTEP representation of the asymmetric unit of NiL[4] (**4**) with thermal ellipsoids shown at the 50% probability level.

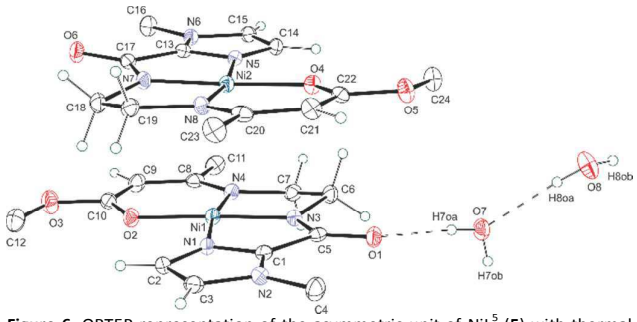

Figure 6. ORTEP representation of the asymmetric unit of NiL[5] (**5**) with thermal ellipsoids shown at the 50% probability level.

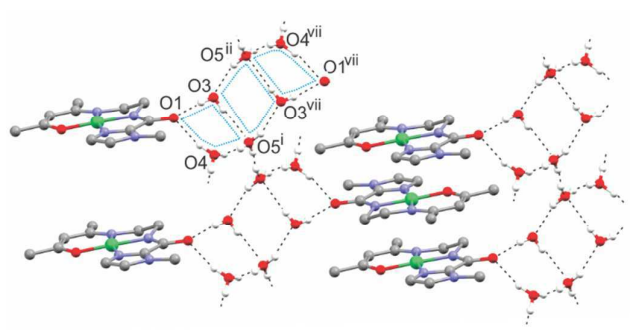

Figure 7. Infused HB rings in complex **4**. Each O4 and O5 atom is bonded to one full occupancy H atom and two partial, 50% occupancy H atoms (see text). HB interactions are denoted by black dashed lines. The thee $R^2_4(8)$ graph sets are noted by the dotted blue lines. Atoms generated by symmetry as marked as follows: i = (x, y, -1+z), ii = (1-x, -y, 1-z), vii = (1-x, -y, -z).

The extended HB in **4** creates a cascade water network. The water molecules are arranged in three $R^2_4(8)$ rings (dotted blue lines) fused together in a stair-step fashion generating a larger $R^8_8(16)$ pattern, Figure 7. Each $R^8_8(16)$ ring is a part of a pair of infinite chains best described as a $C^3_3(6)$ (dotted red line) in the *a*-direction and a $C^5_5(10)$ (dotted green line) along the *b*-direction, Figure 8. The substitution of the methyl substituent in **4** with a methoxy group in **5** results in significant changes in the H-bonding network. In **5**, there are two metal complexes and two waters of hydration in the asymmetric unit. The carboxamido oxygen O1 associated with Ni1 accepts an H-bond from O7. The O7-H7oa···O1 angle is 174(3)° with a D···A distance of 2.775(3) Å and an H···A distance of 2.01(3) Å. The carboxamido oxygen O4 associated with Ni2 is an H-bond acceptor from both O7 and O8 containing water molecules. The O7-H7ob···O4^{i} (1-x, -0.5+y, 0.5-z) angle is 169(4)° with a D···A distance of 2.942(3) Å and an H···A distance of 2.18(4) Å. The O8-H8ob···O4^{ii} (1+x, 1.5-y, 0.5+z) interaction is similar with an angle of 167(3)°, a D···A distance of 2.879(3) Å, and an H···A distance of 2.11(4) Å. Additionally, the O8 containing water molecule acts as an H-bond donor to O7.

Table 3. Selected HB metrics for **1 – 5**.

D-H···A	H···A (Å)	D···A (Å)	D-H···A (°)
1			
O2-H2oa···O1	1.90(5)	2.756(4)	163(5)
O2-H2ob···O2^{i}	1.96(5)	2.892(5)	168(5)
O2-H2oc···O2^{ii}	2.01(5)	2.892(5)	174(5)
N4-H4···S1^{iii}	2.57(4)	3.409(3)	163(4)
symmetry codes: i = (-x, 2-y, 1-z); ii = (-x, 1-y, 1-z); iii = (x, 1+y, z).			
2			
O2-H2oa···O1	1.93(3)	2.818(4)	175(6)
O2-H2ob···O2^{i}	1.92(10)	2.788(5)	169(16)
O2-H2oc···O2^{ii}	1.96(9)	2.794(5)	157(12)
N4-H4···S1^{iii}	2.50(6)	3.417(4)	173(4)
symmetry codes: i = (-x, -y, -z); ii = (-x, 1-y, -z); iii = (x, -1+y, z).			
3			
O2-H2o^{ii}···O1	2.010(18)	2.7979(13)	162.8(19)
N4-H4na···O1^{iii}	2.072(19)	2.9431(17)	173.1(16)
symmetry codes: ii = (0.5-x, y, 1.5-z); iii = (-0.5+x, 1-y, -0.5+z).			
4			
O3-H3oa···O1	1.938(18)	2.720(2)	175(2)
O3-H3ob···O5^{i}	2.09(2)	2.873(3)	178(2)
O4-H4oa···O1	2.01(2)	2.803(3)	173(3)
O4-H4ob···O4^{iii}	1.98(5)	2.765(3)	172(7)
O4-H4oc···O5^{iv}	2.04(3)	2.800(3)	166(6)
O5-H5oa···O3^{ii}	2.04(3)	2.786(3)	160(3)
O5-H5ob···O5^{v}	2.06(6)	2.827(3)	169(7)
O5-H5oc·O4^{vi}	2.08(3)	2.800(3)	154(7)
symmetry codes: i = (x, y, -1+z); ii = (1-x, -y, 1-z); iii = (2-x, 1-y, -z); iv = (x, y, 1+z); v = (2-x, -y, 2-z); vi = (x, y, 1+z).			
5			
O7-H7oa···O1	2.01(3)	2.775(3)	174(3)
O7-H7ob···O4^{i}	2.18(4)	2.942(3)	169(4)
O8-H8oa···O7	2.06(3)	2.871(4)	173(3)
O8-H8ob···O4^{ii}	2.11(4)	2.879(3)	167(3)
symmetry codes: i = (1-x, -0.5+y, 0.5-z); ii = (1+x, 1.5-y, 0.5+z).			

The extended H-bonding in **5** forms isolated pools of water, Figure 9, as a result of the substitution of -CH_3 in **4** with -OCH_3 in **5** results. The methoxy groups serve as a gate to generate isolated void spaces within an ABBA stacking arrangement. The water molecules are arranged in $R^4_6(12)$ rings (dotted blue line) comprised of carboxamido atoms O4 and O4^{iii} (2-x,1-y,1-z) and four water molecules. The rings are anchored between stacks of metal complexes through direct H-bond interactions between O7 and O1. Notably, the methoxy subsitutents (O3-C12) of neighboring stacks are in close contact creating a barrier between adjacent rings of water.

This journal is © The Royal Society of Chemistry 20xx

Please do not adjust margins

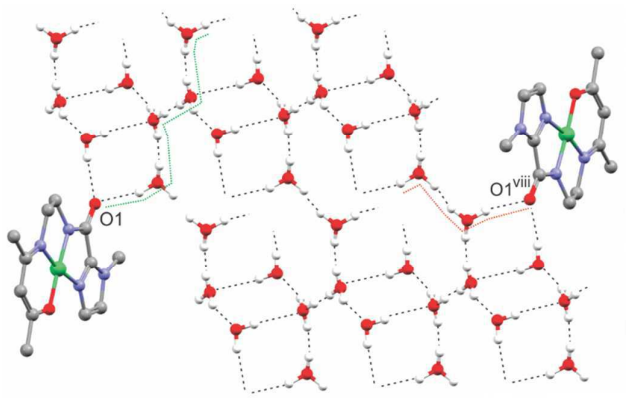

Figure 8. 2D HB water "cascade" in complex **4**. HB interactions are denoted by black dashed lines. Graph sets are noted by dotted colored lines as follows: $C^{3}_{3}(6)$ (red) and $C^{2}_{5}(10)$ (green). Atoms marked with '''' are symmetry generated (4-x, 1-y, -z).

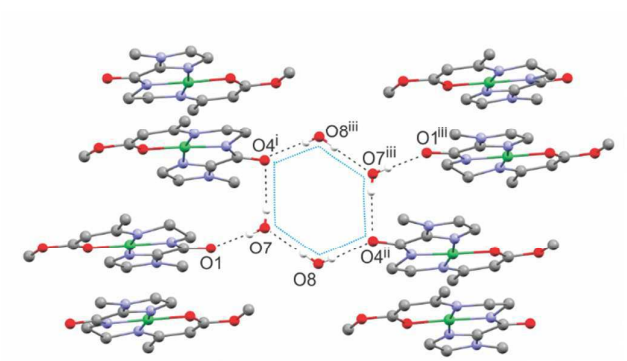

Figure 9. Isolated HB "pool" of water in complex **5**. HB interactions are denoted by black dashed lines. The $R^{4}_{6}(12)$ graph set is noted by the dotted blue line. Atoms generated by symmetry as marked as follows: ' = (1-x, -0.5+y, 0.5-z), '' = (1+x, 1.5-y, 0.5+z), ''' = (2-x, 1-y, 1-z).

Conductivity studies

The electrical impedance of crystals of **1**, **4**, and **5** were evaluated by Electrochemical Impendence Spectroscopy (EIS). No peak (time constant) is observed in the plot of phase angle vs. frequency indicating no Faradaic electrochemical processes occur within crystals at the biases applied (Figure S33).[19] The total impedance, Z, is a combination of real (Z') and imaginary (Z'') contributions.[20] Data for **1**, **4**, and **5** are summarized in Table S2. At high frequency (~100 kHz), the real component represents the system resistance. Under these conditions, Z' values with no applied bias are 730, 650, and 580 Ω for **1**, **4**, and **5**, respectively. The imaginary component involves inductive and capacitive contributions to impedance. The capacitance was determined by fitting measured impedance data to an electrical circuit model using the method of least squares.[21] Several models were evaluated and convergence was only achieved for a capacitor circuit. The capacitance for all three complexes ranges from 1.12×10^{-10} – 1.27×10^{-10} F.

Analysis of the Nyquist representation (Z' and –Z'') for the complexes shows that Z'' changes with frequency, in the high frequency domain, while Z' remains relatively constant (Figure S34). This indicates that the vast majority of the system impedance is caused by capacitive elements, rather than resistive elements.[22] The impedance of an ideal capacitor is inversely proportional to frequency.[20] This trend is observed for the control capacitor (0.22 μF, Sangamo USA), **1**, **4**, and **5** (Figure S33).

The similarities measured capacitances and system resistances for **1**, **4**, and **5** is attributed to the nearly identical π-stacking distances of the metal complexes of ~3.4 Å. Charge transfer appears to propagate through the metal complex stacks with the water of hydration serving a structural role. It is envisioned that the water structure could serve as a conduit for proton conduction, which is a focus of continued efforts.

Thermal analyses

TGA and DSC traces of complexes **1**, **2**, **4**, and **5** are shown in Figures S24 – S31. In complexes **1** and **2**, there is a clear dehydration step beginning near 50 °C with a mass loss of 6.09 and 6.12%, respectively, upon reaching 150 °C. The mass change is consistent with the loss of one water molecule per complex from the lattice. Decomposition of the ligand framework of **1** and **2** occurs above 200 °C and 250 °C, respectively. Degradation is accompanied by a phase transition as indicated by the endothermic process observed by DSC.[23,24] In **4** and **5** dehydration begins at, or below, room temperature and is complete by 70 °C with a mass loss of 14.89% (three water molecules) and 9.698% (two water molecules), respectively. Both **4** and **5** display complete mass loss by 320 °C attributed to sublimation of the complexes, which was confirmed experimentally. A phase transition, as observed by DSC, occurs prior to sublimation.

The HB motif in the hydrated crystals correlates with the temperature range of the dehydration process. For **1** and **2**, the 1D chain requires a higher temperature to break the relatively strong HB interactions within the channel and between the water and structural O atoms. For **4** and **5**, the water motif is more open with a greater variability in the types and strengths of HB interactions. The relatively low temperature required to initiate dehydration suggests that cleavage of the weakest interactions initiates complete dehydration through a breakdown of the HB network. A detailed analysis based on HB distances and angles is not possible due to relatively small changes in HB parameters with respect to their standard deviations, Table 3.

Conclusions

The HB motifs in the related planar Ni(II) complexes **1**, **2**, **4**, and **5** vary as a function of the crystal packing of the host molecules, Scheme 2. The interlayer HB interactions in **1** and **2** results in an AAAA stacking arrangement, which positions the carbonyl O atoms to interact water molecules confined in 1D channels. The absence of HB stacking interactions between the layers of **4** result in an ABAB stacking arrangement with large void spaces between alternating layers. The $–OCH_3$ group in **5** act as a gate to generate isolated void spaces resulting in pools of water as a result of the ABBA stacking arrangement. The mass quantity of water stored per volume of crystal is dependent on the packing arrangement. The pools of **5** contain the least amount of water at 10.96 mg/cm^3. The streams of **1**

and **2** hold approximately twice as much water as **5** with values of 20.72 and 23.97 mg/cm^3, respectively. The cascades of **4** retain 116.7 mg/cm^3, which is 10 times the water of **5**. The capacitances and system resistances are relatively constant for **1**, **4**, and **5** and can be attributed to the nearly identical π-stacking distances of the metal complexes. The HB motifs facilitate orientation of the metal stacks to support propagation of the charge carriers, but do not appear to be directly involved in charge propagation. The thermal properties of the hydrated structures correlate with the differences in the HB motifs. These results offer promise for the rational design of HB motifs based on small changes in the host framework with predictable physical properties.

From a design standpoint the *N*-(2-aminoethyl)-1-methylimidazole-2-carboxamide building block (and related motifs) can be assembled as solids with tunable conductivity. This could be accomplished by varying the ligand backbone or other substituents to modulate the spacing between complexes in the stack. Further, modification of the steric bulk around the carboxamido-O can be used to control the H-bonding motif and dehydration temperatures. The combination of these two effects can be employed to design materials that undergo structural changes upon dehydration with quantifiable effects on the charge transfer properties of the materials. Studies of this type are underway.

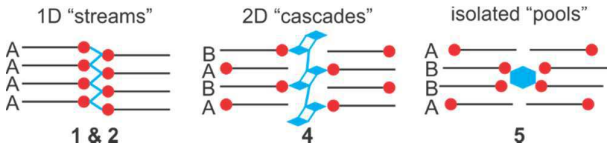

Scheme 2. Stacking arrangements of complexes **1**, **2**, **4**, and **5**.

Experimental

Syntheses

All chemicals were obtained from commercial sources without further purification unless otherwise noted. Reagent-grade solvents were dried using standard operating procedures and degassed under nitrogen atmosphere. Most of the reactions were carried out under an inert atmosphere using standard Schlenk line techniques and a N_2-filled glovebox. The compounds ethyl 1-methylimidazole-2-carboxylate, H_2L^2, and NiL^2 (**1**) were prepared following literature procedures.[16,25]

N-(2-aminoethyl)-1-methyl-1H-imidazole-2-carboxamide (**HL^1**): Ethylenediamine (2.0 ml, 29.9 mmol) was added to a toluene solution of ethyl 1-methylimidazole-2-carboxylate (2.52 g, 16.4 mmol). The reaction mixture was refluxed with a Dean-Stark apparatus for 12-36 hours, whereupon ethanol was removed from the reaction mixture. Volatile components of the solution were removed on a rotary evaporator giving a yellow oil (2.33 g, 84.5% yield). Product formation was confirmed by NMR and infrared spectroscopy. ^{1}H NMR (DMSO): δ 2.05 (br, 2H), 2.63 (t, 2H), 3.28 (t, 2H), 3.98 (s, 3H), 6.82 (d, 1H), 6.88 (d, 1H), 8.14 (s, 1H). FT-IR (ATR), cm^{-1}: 1475 (m), 1505 (m), 1545 (s), 1663 (s).

N'-(mercaptoethyl)-N-(2-aminoethyl)-1-methyl-1H-imidazole-2-carboxamide (**H_2L^3**): This ligand was prepared in a manner analogous to that of H_2L^2. Ethylene sulfide (3.5 ml, 59 mmol) was added via syringe to a degassed benzene solution of HL^1 (1.0 g, 6.0 mmol). The reaction vessel was thoroughly purged with N_2 and then refluxed for 18 hours. Removal of the solvent and excess ethylene sulfide *in vacuo* gave a pale yellow residue (1.16 g, 84.7% yield) of suitable purity. ^{1}H NMR (C_6D_6): δ 1.35 (br, 1H), 2.3-2.7 (m, 6H), 3.2-3.5 (m, 3H), 3.68 (s, 3H), 6.32 (d, 1H), 6.92 (d, 1H), 8.08 (s, 1H).

NiL^3 (**2**): A degassed green benzene solution (30 ml) of $Ni(acac)_2$ (0.918 g, 3.57 mmol) was slowly added via cannula to a pale yellow solution of H_2L^3 (1.16 g, 5.08 mmol) of equal volume over a 1-2 hour period. During the course of addition, the color of the solution changed to a deep red, followed by precipitation of a red solid upon overnight stirring. The reaction mixture was filtered and the crude product was loaded onto an alumina column as an acetonitrile solution. The pure product was isolated as a red band after elution with 3:1 acetonitrile/methanol. X-ray quality single crystals (0.52 g, 51.6%) were grown upon evaporation of a methanol solution. Anal. Calcd. for $C_9H_{14}N_4OSNi{\cdot}H_2O$: C, 35.67; H, 5.32; N, 18.49. Found: C, 35.74; H, 4.98; N, 18.45. +MALDI, m/z calcd for {[NiL^3]-H$^+$} 285.023; Found 285.188. ^{1}H NMR (CD_3OD): δ 1.18 (s, 1H), 2.16-3.45 (m, 8H), 3.78 (s, 3H), 6.29 (d, 1H), 6.92 (d, 1H). FT-IR (ATR), cm^{-1}: 1443 (m), 1636 (s). Electronic absorption (CH_3CN (22 °C)): λ_{max} (nm) (ε (cm^{-1} M^{-1})) 368 (1075), 449 (135), 575 (45).

$Ni(L^1)_2$ (**3**): A dry green toluene (20 ml) solution of $Ni(acac)_2$ (0.85 g, 3.3 mmol) was added slowly via cannula to a toluene solution (18 ml) of HL^1 (0.65 g, 3.9 mmol). Upon complexation, a pale blue precipitate began to form, which appeared to become greener in color as more nickel was added. The light blue solid that precipitated upon overnight stirring was separated from the yellow supernatant by anaerobic filtration. Upon anaerobic washing with two 50 mL portions of dry toluene, the acetylacetone by-product was removed, yielding the faint blue product. Upon drying under vacuum, the crude product was attained (0.70 g, 92% yield). Recrystallization from evaporation of an acetonitrile solution gave blue crystals. +MALDI, m/z calcd for {[$Ni(L^1)_2$]-H$^+$} 393.121; Found 393.286. FT-IR (ATR), cm^{-1}: 1478 (m), 1597 (s), 3235-3275 (m). Electronic absorption (CH_2Cl_2 (22 °C)): λ_{max} (nm) (ε (cm^{-1} M^{-1})) 319 (1110), 488 (75), 980 (85).

NiL^4(**4**): The ligand HL^4 was prepared via a metal-templated route. A 1:1 mixture of acetone/water (10 ml) was added to a crude **3** (0.15 g, 0.38 mmol). The reaction mixture was exposed to atmosphere for 24 hours, resulting in the formation of an orange solution. Evaporative crystallization of the acetone/water solution gave x-ray quality orange single crystals. Isolation of pure NiL^4 was achieved by washing the crystalline product with water and diethyl ether, respectively (0.053 g, 43% yield). Anal. Calcd. for $C_{12}H_{16}N_4O_2Ni$: C, 46.95; H, 5.25; N, 18.25. Found: C, 46.71; H, 5.17; N, 18.03. +MALDI, m/z calcd for {[NiL^4]-H$^+$} 307.062; Found 307.253. ^{1}H NMR (C_3D_6O):

This journal is © The Royal Society of Chemistry 20xx

δ 1.77 (s, 3H), 1.90 (s, 3H), 2.84 (t, 2H), 3.41 (t, 2H), 3.92 (s, 3H), 4.98 (s, 1H), 6.61 (d, 1H), 7.05 (d, 1H). FT-IR (ATR), cm^{-1}: 1500 (s), 1510 (s), 1590 (m), 1610 (s), 2850 (w), 2930 (w), 3120 (w). Electronic absorption (CH_3CN (22 °C)): λ_{max} (nm) (Ɛ (cm^{-1} M^{-1})) 216 (754), 324 (580), 426 (168), 508 (108).

NiL[5] (**5**): Complex **3** (0.40 g, 1.02 mmol) was dissolved in 25 mL of DI water and methyl acetoacetate (0.110 mL, 1.02 mmol) was then added. The solution was allowed to stir for 24 hours resulting in an orange solution. The solvent was removed via rotary evaporation yielding an orange solid (0.24 g, 72.8 % yield). Orange plate crystals suitable for x-ray analysis were obtained by slow evaporation of acetonitrile solution. Anal. Calcd. for $C_{12}H_{16}N_4O_3Ni{\cdot}3H_2O$: C, 38.23; H, 5.88; N, 14.86. Found: C, 38.49; H, 5.72; N, 15.34. +MALDI, m/z calcd for $[NiL^5]^+$ 322.657; Found 322.978. ^1H NMR ($CDCl_3$): δ 1.78 (s, 3H), 1.82 (s, 3H), 2.92 (t, 2H), 3.45 (t, 3H), 3.88 (s, 3H), 4.86 (s, 1H), 6.62 (d, 1H), 6.64 (d, 1H). FT-IR (ATR),cm^{-1} : 1050 (m), 1500 (s), 1585 (m), 1625 (s), 2835 (w), 2916 (w), 3085 (w). Electronic absorption (CH_3CN (22 °C)): λ_{max} (nm) (Ɛ (cm^{-1} M^{-1})) 209 (620), 250 (565), 305 (530), 380 (85), 475 (32).

Physical measurements

Elemental analyses were performed by Midwest Microlab (Indianapolis, IN). IR spectra were recorded on a Thermo Nicolet Avatar 360 spectrometer with ATR attachment (4 cm^{-1} resolution). Matrix Assisted Laser Desorption/Ionization (MALDI) was collected by Voyager Biospectrometry DE Workstation (Applied Biosystems, Foster City, CA, USA) and processed by Data Explorer Software TM (Version 4.8) at University of Louisville. The matrix for MALDI experiment was prepared by dissolving 0.18 M Paranitroaniline (PNA) in 1:1 MeOH:$CHCl_3$ solution. The samples were dissolved in methanol and 0.75 ml aliquot using the dried-droplet method. Electronic absorption spectra were recorded with an Agilent 8453 diode array spectrometer with a 1 cm path length quartz cell. NMR spectra were obtained on a Varian Inova 400 MHz spectrometer.

A Metrohm Autolab PGSTAT302N potentiostat/galvanostat, operating in potentiostat mode was used to collect the electrochemical impedance spectroscopy (EIS) measurements. A DC bias of -0.1, 0, or 0.1 V was applied throughout EIS measurements with an amplitude of 10 mV_{RMS} over the frequency range 100 kHz to 10 Hz. TGA and DSC of the complexes were performed at the Conn Center for Renewable Energy Research, using an SDT Q600 TA analyzer. The sample pan was loaded with 15 - 20 mg of sample for each run. Data points were collected at a ramp rate of 2°C/min in a flowing (100 ml/min) N_2 stream.

Single crystal x-ray structure determination

An orange cube 0.25 x 0.25 x 0.25 mm^3 crystal of **2** was mounted on a glass fiber for collection of x-ray data on a Bruker SMART APEX CCD diffractometer. The SMART[26] software package (v 5.632) was used to acquire a total of 1,868 thirty-second frame ω-scan exposures of data at 100K to a $2\Theta_{max}$ = 56.10° using monochromated MoKα radiation (0.71073 Å) from a sealed tube and a monocapillary. Frame data were integrated using SAINT[27] (v 6.45) to a theta max diffraction limit of 25.12° and processed to determine final unit cell parameters: a = 11.9515(15) Å, b = 4.8375(6) Å, c = 22.198(3) Å, β= 103.424(2)°, V = 1248.3(3) $Å^3$, D_{calc} = 1.612 Mg/m^3, Z = 4 to produce raw hkl data that were then corrected for absorption (transmission min./max. = 1.00/0.636; μ = 1.717 mm^{-1}) using SADABS[28] (v 2.10). The structure was solved by Patterson methods in the space group $P2_1/c$ using SHELXS[29] and refined by least squares methods on F^2 using SHELXL[29] incorporated into the SHELXTL[30] (v 6.14) suite of programs. All non-hydrogen atoms were refined with anisotropic atomic displacement parameters. All hydrogen atoms (except methyl H's) were located by difference maps and refined isotropically. Methyl hydrogen atoms were placed in their geometrically generated positions and refined as a riding model; methyl groups were allowed to ride (the torsion angle which defines its orientation was allowed to refine) on the attached C atom, and these atoms were assigned U(H) = 1.5 x Ueq. The water of hydration is modeled with a full occupancy oxygen, O2, one full occupancy hydrogen, H2oa and a positionally disordered hydrogen atom modeled with 50% occupancy each for H2ob and H2oc (each refined isotropically with minimal restraints). For all 2,227 unique, reflections (R(int) 0.036) the final anisotropic full matrix least-squares refinement on F^2 for 210 variables converged at R1 = 0.047 and wR2 = 0.116 with a GOF of 1.08.

Crystals of **3** suitable for x-ray analysis were grown by slow evaporation of acetonitrile soln. X-ray structural analysis for **3** was performed on a 0.35 x 0.33 x 0.30 mm^3 blue prism using an identical data acquisition strategy described above for **2** at 100 K to a $2\Theta_{max}$ = 56.30° and processed to a theta max diffraction limit of 25.08°. Complex **3** crystallizes in the space group P2/n with unit cell parameters: a = 9.1756(19) Å, b = 10.590(2) Å, c = 9.4434(19) Å, β= 98.876(3)°, V = 906.7(3) $Å^3$, Z = 2 and D_{calc} = 1.506 Mg/m^3. 1621 raw independent data were corrected for absorption (transmission min./max. = 0.571/0.715; μ = 1.103 mm-^{1}) using SADABS. The structure was solved by Patterson methods using SHELXTL[30]. All non-hydrogen atoms were refined with anisotropic atomic displacement parameters. All hydrogen atoms (except methyl H's) were located by difference maps and refined isotropically. Methyl H's were included as fixed contributions as described above for **2**. For all 1,621 unique reflections (R(int) 0.0141) the final anisotropic full matrix least-squares refinement on F^2 for 155 variables converged at R1 = 0.0222 and wR2 = 0.0569 with a GOF of 1.008.

An orange needle 0.50 x 0.03 x 0.01 mm^3 crystal of **4** grown from an acetone/water solution was mounted on a 0.05 mm CryoLoop with Paratone oil for collection of x-ray data on a Bruker SMART APEX CCD diffractometer using an identical data acquisition strategy described above for **2** at 100 K to a $2\Theta_{max}$ = 55.98°. Frame data were processed to a theta max diffraction limit of 25.11° using SAINT[27] (v 6.45) to determine final unit cell parameters: a = 6.8975(18) Å, b = 9.130(2) Å, c = 12.645(3) Å, α = 92.821(4)°, β = 92.276(4)°, γ = 104.339(4)°, V = 769.4(3) $Å^3$, D_{calc} = 1.558 Mg/m^3, Z = 2 to produce raw hkl data that were then corrected for absorption (transmission min./max. = 0.613/0.871; μ= 1.290 mm^{-1}) using SADABS[28] (v 2.10). The

structure was solved by Direct methods using SHELXTL[30]. All non-hydrogen atoms were refined with anisotropic atomic displacement parameters. All hydrogen atoms (except methyl H's) were located by difference maps and refined isotropically. The structural model contains two disordered waters of hydration that are modeled as follows. O4 is a full occupancy oxygen refined anisotropically with one full occupancy hydrogen, H4oa and a positionally disordered hydrogen atom modeled with 50% occupancy each for H4ob and H4oc (each refined isotropically with minimal sadi restraints). The water comprised of O5, H5oa, H5ob and H5oc was modelled similarly. For all 2,709 unique reflections (R(int) = 0.0231) the final anisotropic full matrix least-squares refinement on F^2 for 257 variables converged at R1 = 0.0356 and wR2 = 0.0588 with a GOF of 1.052.

Crystals of **5** suitable for x-ray analysis were grown by slow evaporation of acetonitrile solution. An orange plate 0.24 x 0.14 x 0.03 mm^3 crystal was mounted on a 0.05 mm CryoLoop with Paratone oil for collection of x-ray data on a Bruker SMART APEX CCD diffractometer using an identical data acquisition strategy described above for **2** at 100 K to a $2\Theta_{max}$ = 56.08° and processed to a theta max diffraction limit of 25.12°. Complex **5** crystallizes in the space group $P2_1/c$ with unit cell parameters: a = 9.2792(6) Å, b = 13.6005(8) Å, c = 21.7240(13) Å, β= 95.3700(10) °, V = 2729.6(3) $Å^3$, Z = 8 and D_{calc} = 1.660 Mg/m^3. 4,861 raw independent data were corrected for absorption (transmission min./max. = 0.754/1.00; μ= 1.444 mm^{-1}) using SADABS. The structure was solved by Patterson methods using SHELXTL[30]. All non-hydrogen atoms were refined with anisotropic atomic displacement parameters. All hydrogen atoms (except methyl H's) were located by difference maps and refined isotropically. Methyl H's were included as fixed contributions as described above for **2**. For all 4,861 unique reflections (R(int) 0.0435) the final anisotropic full matrix least-squares refinement on F^2 for 452 variables converged at R1 = 0.0561 and wR2 = 0.0628 with a GOF of 1.057.

Conflicts of interest

Authors declare no conflicts of interest.

Acknowledgements

This research was supported by the National Science Foundation CHE-1665136. MSM thanks the Department of Energy (DEFG02-08CH11538) and the Kentucky Research Challenge Trust Fund for upgrade of our X-ray facilities. The authors thank Professor Gautum Gupta in the Department of Chemical Engineering for helpful discussions and assistance with analysis of impedance data.

Notes and references

1. (a) M. Gladovic, U. Bren and T. Urbic, *Mol. Phys.*, 2018, **116**, 1133-1144; (b) P. Gallo, K. Amann-Winkel, C. A. Angell, M. A. Anisimov, F. Caupin, C. Chakravarty, E. Lascaris, T. Loerting, A. Z. Panagiotopoulos, J. Russo, J. A. Sellberg, H. E. Stanley, H. Tanaka, C. Vega, L. Xu and L. G. M. Pettersson, *Chem. Rev.*, 2016, **116**, 7463-7500; (c) S. Cerveny, F. Mallamace, J. Swenson, M. Vogel and L. Xu, *Chem. Rev.*, 2016, **116**, 7608-7625; (d) O. Björneholm, M. H. Hansen, A. Hodgson, L. M. Liu, D. T. Limmer, A. Michaelides, P. Pedevilla, J. Rossmeisl, H. Shen, G. Tocci, E. Tyrode, M. M. Walz, J. Werner and H. Bluhm, *Chem. Rev.*, 2016, **116**, 7698-7726; (e) M. C. Bellissent-Funel, A. Hassanali, M. Havenith, R. Henchman, P. Pohl, F. Sterpone, D. van der Spoel, Y. Xu and A. E. Garcia, *Chem. Rev.*, 2016, **116**, 7673-7697; (f) M. Ceriotti, W. Fang, P. G. Kusalik, R. H. McKenzie, A. Michaelides, M. A. Morales and T. E. Markland, *Chem. Rev.*, 2016, **116**, 7529-7550; (g) G. A. Cisneros, K. T. Wikfeldt, L. Ojamäe, J. Lu, Y. Xu, H. Torabifard, A. P. Bartók, G. Csányi, V. Molinero and F. Paesani, *Chem. Rev.*, 2016, **116**, 7501-7528; (h) M. Monasterio, J. J. Gaitero, H. Manzano, J. S. Dolado and S. Cerveny, *Langmuir*, 2015, **31**, 4964-4972; (i) R. Alenka, L. N. Zabukovec, H. S. K. and K. Venčeslav, *Adv. Funct. Mater.*, 2012, **22**, 1952-1957; (j) P. Demontis, J. Gulín-González, M. Masia and G. B. Suffritti, *J. Phys.: Condens. Matter.*, 2010, **22**, 284106.

2. L. Fumagalli, A. Esfandiar, R. Fabregas, S. Hu, P. Ares, A. Janardanan, Q. Yang, B. Radha, T. Taniguchi, K. Watanabe, G. Gomila, K. S. Novoselov and A. K. Geim, *Science*, 2018, **360**, 1339-1342.

3. (a) A. Dey, D. Bairagi and K. Biradha, *Cryst. Growth Des.*, 2017, **17**, 3885-3892; (b) H. X. Zhao, X. J. Kong, H. Li, Y. C. Jin, L. S. Long, X. C. Zeng, R. B. Huang and L. S. Zheng, *PNAS*, 2011, **108**, 3481-3486; (c) H. B. Xiong, D. Sun, G. G. Luo, R. B. Huang and J. C. Dai, *J. Mol. Struct.*, 2011, **990**, 164-168; (d) S. Kohmoto, S. Okuyama, N. Yokota, M. Takahashi, K. Kishikawa, H. Masu and I. Azumaya, *Cryst. Growth Des.*, 2011, **11**, 3698-3702; (e) N. Ramalingam, J. P. H. Charmant, A. G. Orpen and A. P. Davis, *Angew. Chem. Int. Ed.*, 2010, **49**, 5125-5129; (f) X. F. Shi, H. B. Song, L. He and W. Q. Zhang, *CrystEngComm*, 2009, **11**, 542-544; (g) Y. Cui, M. L. Cao, L. F. Yang, Y. L. Niu and B. H. Ye, *CrystEngComm*, 2008, **10**, 1288-1290; (h) M. Tadokoro, S. Fukui, T. Kitajima, Y. Nagao, S. I. Ishimaru, H. Kitagawa, K. Isobe and K. Nakasuji, *Chem. Commun.*, 2006, **0**, 1274-1276; (i) F. Li, T. Li, D. Yuan, J. Lv and R. Cao, *Inorg. Chem. Commun.*, 2006, **9**, 691-694; (j) B. K. Saha and A. Nangia, *Chem. Commun.*, 2005, **0**, 3024-3026; (k) Q. Y. Liu and L. Xu, *CrystEngComm*, 2005, **7**, 87-89; (l) R. Carballo, B. Covelo, C. Lodeiro and E. M. Vazquez-Lopez, *CrystEngComm*, 2005, **7**, 294-296; (m) S. Banerjee and R. Murugavel, *Cryst. Growth Des.*, 2004, **4**, 545-552; (n) L. E. Cheruzel, M. S. Pometun, M. R. Cecil, M. S. Mashuta, R. J. Wittebort and R. M. Buchanan, *Angew. Chem. Int. Ed.*, 2003, **42**, 5452-5455.

4. (a) L. Yang-Hui, W. Dong-En, W. Gao-Ju, G. Lian-Shuai, C. Lan, W. Jin-Wen and S. Bai-Wang, *ChemistrySelect*, 2017, **2**, 61-64; (b) S. Upreti, A. Datta and A. Ramanan, *Cryst. Growth Des.*, 2007, **7**, 966-971; (c) X. Luan, Y. Chu, Y. Wang, D. Li, P. Liu and Q. Shi, *Cryst. Growth Des.*, 2006, **6**, 812-814; (d) R. Carballo, B. Covelo, N. Fernández-Hermida, E. García-Martínez, A. B. Lago, M. Vázquez and

 This journal is © The Royal Society of Chemistry 20xx

E. M. Vázquez-López, *Cryst. Growth Des.*, 2006, **6**, 629-631; (e) P. S. Lakshminarayanan, E. Suresh and P. Ghosh, *J. Am. Chem. Soc.*, 2005, **127**, 13132-13133; (f) Z. Fei, T. J. Geldbach, D. Zhao, R. Scopelliti and P. J. Dyson, *Inorg. Chem.*, 2005, **44**, 5200-5202; (g) C. Janiak, T. G. Scharmann and S. A. Mason, *J. Am. Chem. Soc.*, 2002, **124**, 14010-14011.

5. (a) A. Akaishi, T. Yonemaru and J. Nakamura, *ACS Omega*, 2017, **2**, 2184-2190; (b) C. Perez, D. P. Zaleski., N. A. Seifert, B. Temelso, G. C. Shields, Z. Kisiel and B. H. Pate, *Angew. Chem. Int. Ed.*, 2014, **53**, 14368-14372; (c) C. M. Jin, Z. Zhu, Z. F. Chen, Y. J. Hu and X. G. Meng, *Cryst. Growth Des.*, 2010, **10**, 2054-2056; (d) A. H. Yang, H. Zhang, H. L. Gao, W. Q. Zhang, L. He and J. Z. Cui, *Cryst. Growth Des.*, 2008, **8**, 3354-3359; (e) C. H. Li, K. L. Huang, J. M. Dou, Y. N. Chi, Y. Q. Xu, L. Shen, D. Q. Wang and C. W. Hu, *Cryst. Growth Des.*, 2008, **8**, 3141-3143; (f) X. F. Shi and W. Q. Zhang, *Cryst. Growth Des.*, 2007, **7**, 595-597; (g) Y. G. Huang, Y. Q. Gong, F. L. Jiang, D. Q. Yuan, M. Y. Wu, Q. Gao, W. Wei and M. C. Hong, *Cryst. Growth Des.*, 2007, **7**, 1385-1387; (h) S. R. Choudhury, A. D. Jana, E. Colacio, H. M. Lee, G. Mostafa and S. Mukhopadhyay, *Cryst. Growth Des.*, 2007, **7**, 212-214; (i) B. K. Saha and A. Nangia, *Chem. Commun.*, 2006, **0**, 1825-1827; (j) D. L. Reger, R. F. Semeniuc, C. Pettinari, F. Luna-Giles and M. D. Smith, *Cryst. Growth Des.*, 2006, **6**, 1068-1070; (k) M. Li, S. Chen, J. Xiang, H. He, L. Yuan and J. Sun, *Cryst. Growth Des.*, 2006, **6**, 1250-1252; (l) X. M. Zhang, R. Q. Fang and H. S. Wu, *Cryst. Growth Des.*, 2005, **5**, 1335-1337; (m) J. P. Zhang, Y. Y. Lin, X. C. Huang and X. M. Chen, *Inorg. Chem.*, 2005, **44**, 3146-3150; (n) J. Lu, J. H. Yu, X. Y. Chen, P. Cheng, X. Zhang and J. Q. Xu, *Inorg. Chem.*, 2005, **44**, 5978-5980; (o) Y. Bao-Hui, S. Ai-Ping, W. Tong-Fei, W. Yan-Qin and C. Xiao-Ming, *Eur. J. Inorg. Chem.*, 2005, **2005**, 1230-1234; (p) B. Q. Ma, H. L. Sun and S. Gao, *Chem. Commun.*, 2004, **0**, 2220-2221; (q) S. Bellam and V. J. J, *Angew. Chem. Int. Ed.*, 2004, **43**, 5769-5772.

6. (a) F. G. Vogt, J. Brum, L. M. Katrincic, A. Flach, J. M. Socha, R. M. Goodman and R. C. Haltiwanger, *Cryst. Growth Des.*, 2006, **6**, 2333-2354; (b) L. Yu, *Adv. Drug Del. Rev.*, 2001, **48**, 27-42.

7. (a) A. Akaishi, T. Yonemaru and J. Nakamura, *ACS Omega*, 2017, **2**, 2184-2190; (b) O. Z. Yesilel, H. Erer and O. Buyukgungor, *CrystEngComm*, 2011, **13**, 1339-1349; (c) H. J. Hao, D. Sun, F. J. Liu, R. B. Huang and L. S. Zheng, *Cryst. Growth Des.*, 2011, **11**, 5475-5482; (d) R. L. Sang and L. Xu, *CrystEngComm*, 2010, **12**, 1377-1381; (e) S. Mandal, A. Castineiras, T. K. Mondal, A. Mondal, D. Chattopadhyay and S. Goswami, *Dalton Trans.*, 2010, **39**, 9514-9522; (f) W. Z. Xu, J. Sun, Z. T. Huang and Q. Y. Zheng, *Chem. Commun.*, 2009, **0**, 171-173; (g) Y. Bi, W. Liao, H. Zhang and D. Li, *CrystEngComm*, 2009, **11**, 1213-1216; (h) P. Qinhe, L. Jiyang, C. K. E., B. Charlotte, R. Xiaoyan, S. Lei, S. Junliang, Z. Xiaodong, L. Guanghua, Y. Jihong and X. Ruren, *Angew. Chem. Int. Ed.*, 2008, **47**, 7868-7871; (i) F. Dai, H. He and D. Sun, *J. Am. Chem. Soc.*, 2008, **130**, 14064-14065; (j) M. C. Das. and P. K. Bharadwaj., *Eur. J. Inorg. Chem.*, 2007, **2007**, 1229-1232; (k) L. Cheng, J. B. Lin, J. Z. Gong, A. P. Sun, B. H. Ye and X. M. Chen, *Cryst. Growth Des.*, 2006, **6**, 2739-2746; (l) S. K. Ghosh, J. Ribas, M. S. El Fallah and P. K. Bharadwaj, *Inorg. Chem.*, 2005, **44**, 3856-3862; (m) L. Infantes, J. Chisholm and S. Motherwell, *CrystEngComm*, 2003, **5**, 480-486; (n) L. Infantes and S. Motherwell, *CrystEngComm*, 2002, **4**, 454-461; (o) J. L. Atwood, L. J. Barbour, T. J. Ness, C. L. Raston and P. L. Raston, *J. Am. Chem. Soc.*, 2001, **123**, 7192-7193; (p) L. J. Barbour, G. W. Orr and J. L. Atwood, *Nature*, 1998, **393**, 671-673.

8. (a) K. Roztocki, M. Lupa, A. Sławek, W. Makowski, I. Senkovska, S. Kaskel and D. Matoga, *Inorg. Chem.*, 2018, **57**, 3287-3296; (b) H. Furukawa, F. Gándara, Y.-B. Zhang, J. Jiang, W. L. Queen, M. R. Hudson and O. M. Yaghi, *J. Am. Chem. Soc.*, 2014, **136**, 4369-4381.

9. W. D. Weng, Y. Q. Zheng, H. L. Zhu and J. Q. Xu, *J. Cluster Sci.*, 2015, **26**, 1833-1843.

10. K. Fucke and J. W. Steed, *Water*, 2010, **2**, 333-350.

11. (a) M. Foroutan, S. M. Fatemi and F. Esmaeilian, *Eur. Phys. J. E*, 2017, **40**, 19; (b) V. Buch, *J. Phys. Chem. B*, 2005, **109**, 17771-17774.

12. (a) K. Gerwert, E. Freier and S. Wolf, *Biochim. Biophys. Acta*, 2014, **1837**, 606-613; (b) B. Draghici, D. Vullo, S. Akocak, E. A. Walker, C. T. Supuran and M. A. Ilies, *Chem. Commun.*, 2014, **50**, 5980-5983; (c) H. R. Xu, Q. C. Zhang, H. X. Zhao, L. S. Long, R. B. Huang and L. S. Zheng, *Chem. Commun.*, 2012, **48**, 4875-4877; (d) R. Carrozzo, T. Rizza, S. Lucioli, R. Pierini, E. Bertini and F. M. Santorelli, *Acta Paediatr.*, 2004, **93**, 65-67; (e) A. Peter, L. S. King, Y. Masato, W. B. Guggino, O. P. Ottersen, F. Yoshinori, E. Andreas and N. Søren, *J. Physiol.*, 2002, **542**, 3-16; (f) K. M. Jude, S. K. Wright, C. Tu, D. N. Silverman, R. E. Viola and D. W. Christianson, *Biochemistry*, 2002, **41**, 2485-2491; (g) W. Junfeng, K. Sanguk, K. Frank and C. T. A., *Protein Sci.*, 2001, **10**, 2241-2250; (h) P. Pohl, S. M. Saparov, M. J. Borgnia and P. Agre, *PNAS*, 2001, **98**, 9624-9629; (i) H. Kandori, *Biochim. Biophys. Acta*, 2000, **1460**, 177-191; (j) S. Cukierman, *Biophys. J.*, 2000, **78**, 1825-1834; (k) J. K. Lanyi, *Biochim. Biophys. Acta*, 2000, **1460**, 1-3; (l) R. J. Law., L. R. Forrest., K. M. Ranatunga., P. L. Rocca, D. P. Tieleman and M. S. P. Sansom., *Proteins: Struct., Funct., Bioinf.*, 2000, **39**, 47-55; (m) C. Wang, R. A. Lamb and L. H. Pinto, *Biophys. J.*, 1995, **69**, 1363-1371; (n) G. M. Preston, T. P. Carroll, W. B. Guggino and P. Agre, *Science*, 1992, **256**, 385-387.

13. (a) Y. Matsuki, M. Iwamoto, K. Mita, K. Shigemi, S. Matsunaga and S. Oiki, *J. Am. Chem. Soc.*, 2016, **138**, 4168-4177; (b) Z. Cao, Y. Peng, T. Yan, S. Li, A. Li and G. A. Voth, *J. Am. Chem. Soc.*, 2010, **132**, 11395-11397; (c) G. Hummer, J. C. Rasaiah and J. P. Noworyta, *Nature*, 2001, **414**, 188-190.

14. (a) D. Dong, W. Zhang, A. C. T. van Duin and D. Bedrov, *J. Phys. Chem. Lett.*, 2018, **9**, 825-829; (b) Y. Hori, T. Chikai, T. Ida and M. Mizuno, *PCCP*, 2018, **20**, 10311-10318; (c) S. B. Tayade, S. S. Bhat, R. Illathvalappil, V. M. Dhavale, V. A. Kawade, A. S. Kumbhar, S. Kurungot and C. Nather, *CrystEngComm*, 2018, **20**, 1094-1100; (d) S. Yan, L. Yao, B. Kang and J. Y. Lee, *Comput. Biol. Chem.*, 2016, **65**, 140-147; (e) S. Cukierman, *Biochim. Biophys. Acta*, 2006, **1757**, 876-885; (f) R. Pomès and B. Roux, *Biophys. J.*, 2002, **82**, 2304-2316; (g) N. Agmon, *Chem. Phys. Lett.*, 1995, **244**, 456-462.

15. (a) F. Mouhat, S. Sorella, R. Vuilleumier, A. M. Saitta and M. Casula, *J. Chem. Theory Comput.*, 2017, **13**, 2400-2417; (b) J. A. Tan, J. W. Li, C. C. Chiu, H. Y. Liao, H. T. Huynh and J. L. Kuo, *PCCP*, 2016, **18**, 30721-30732; (c) H. Takahashi,

H. Ohno, T. Yamauchi, R. Kishi, S. I. Furukawa, M. Nakano and N. Matubayasi, *J. Chem. Phys.*, 2008, **128**, 064507; (d) M. Eigen., *Angew. Chem., Int. Ed. Engl.*, 1964, **3**, 1-19.

16. C. S. Mullins, C. A. Grapperhaus, B. C. Frye, L. H. Wood, A. J. Hay, R. M. Buchanan and M. S. Mashuta, *Inorg. Chem.*, 2009, **48**, 9974-9976.
17. M. C. Etter, J. C. MacDonald and J. Bernstein, *Acta Crystallogr., Sect. B: Struct. Sci.*, 1990, **46**, 256-262.
18. L. J. Farrugia, *J. Appl. Crystallogr.*, 2012, **45**, 849-854.
19. J. Huang, Z. Li, B. Y. Liaw and J. Zhang, *J. Power Sources*, 2016, **309**, 82-98.
20. J. R. Macdonald and E. Barsoukov, *History*, 2005, **1**, 1-13
21. D. Johnson, *Inc., Southern Pines, NC*, 2002, **200**.
22. R. Kötz and M. Carlen, *Electrochim. Acta*, 2000, **45**, 2483-2498.
23. Y. Roos and M. Karel, *Biotechnol. Prog.*, 1990, **6**, 159-163.
24. L. Yu, *Adv. Drug Deliv. Rev.,* 2001, **48**, 27-42.
25. K. Krowicki and J. W. Lown, *J. Org. Chem.*, 1987, **52**, 3493-3501.
26. SMART (v 5.632), Bruker AXS Inc., Madison, WI, 2005.
27. SAINT (v 6.45), Bruker AXS Inc., Madison, WI, 2003.
28. G. M. Sheldrick, SADABS (v 2.10), University of Göttingen, Göttingen, Germany, 1994.
29. G. M. Sheldrick, *Acta Crystallogr., Sect. A: Found. Crystallogr.*, 2008, **A64**, 112-122.
30. G. M. Sheldrick, SHELXTL (v 6.14), Bruker AXS Inc., Madison, WI, 2004

This journal is © The Royal Society of Chemistry 20xx

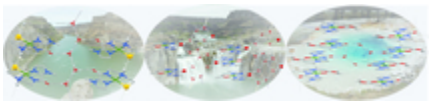

18x4mm (300 x 300 DPI)